







Clouds will Likely Prevent the Detection of Water Vapor in *JWST* Transmission Spectra of Terrestrial Exoplanets

Thaddeus D. Komacek¹ , Thomas J. Fauchez^{2,3,4} , Eric T. Wolf^{5,6} , and Dorian S. Abbot¹ 

¹Department of the Geophysical Sciences, The University of Chicago, Chicago, IL, 60637, USA; tkomacek@uchicago.edu

²NASA Goddard Space Flight Center, Greenbelt, MD, 20771, USA

³Goddard Earth Sciences Technology and Research (GESTAR), Universities Space Research Association, Columbia, MD, USA

⁴GSFC Sellers Exoplanet Environments Collaboration, USA

⁵Laboratory for Atmospheric and Space Physics, Department of Atmospheric and Oceanic Sciences, University of Colorado, Boulder, CO 80309, USA

⁶NASA Astrobiology Institute's Virtual Planetary Laboratory, P.O. Box 351580, Seattle, WA 98195, USA

Received 2019 November 18; revised 2019 December 9; accepted 2019 December 14; published 2020 January 9

Abstract

We are on the verge of characterizing the atmospheres of terrestrial exoplanets in the habitable zones of M dwarf stars. Due to their large planet-to-star radius ratios and higher frequency of transits, terrestrial exoplanets orbiting M dwarf stars are favorable for transmission spectroscopy. In this work, we quantify the effect that water clouds have on the amplitude of water vapor transmission spectral features of terrestrial exoplanets orbiting M dwarf stars. To do so, we make synthetic transmission spectra from general circulation model (GCM) experiments of tidally locked planets. We improve upon previous work by considering how varying a broad range of planetary parameters affects transmission spectra. We find that clouds lead to a 10–100 times increase in the number of transits required to detect water features with the *James Webb Space Telescope (JWST)* with varying rotation period, incident stellar flux, surface pressure, planetary radius, and surface gravity. We also find that there is a strong increase in the dayside cloud coverage in our GCM simulations with rotation periods $\gtrsim 12$ days for planets with Earth's radius. This increase in cloud coverage leads to even stronger muting of spectral features for slowly rotating exoplanets orbiting M dwarf stars. We predict that it will be extremely challenging to detect water transmission features in the atmospheres of terrestrial exoplanets in the habitable zone of M dwarf stars with *JWST*. However, species that are well-mixed above the cloud deck (e.g., CO_2 and CH_4) may still be detectable on these planets with *JWST*.

Unified Astronomy Thesaurus concepts: [Exoplanet atmospheres \(487\)](#); [Exoplanet atmospheric composition \(2021\)](#); [Extrasolar rocky planets \(511\)](#); [Habitable planets \(695\)](#); [Planetary atmospheres \(1244\)](#); [Water vapor \(1791\)](#)

1. Introduction

The upcoming launch of *James Webb Space Telescope (JWST)* and the future space mission concepts LUVOIR/HabEx/OST promise the characterization of terrestrial exoplanet atmospheres. Previous 1D simulations, which cannot properly account for clouds, have indicated that *JWST* will be able to observe the atmospheres of potentially habitable exoplanets orbiting M dwarf stars and detect molecular signatures of life in these atmospheres (Barstow & Irwin 2016; Morley et al. 2017; Lincowski et al. 2018, 2019; Lustig-Yaeger et al. 2019). However, clouds and hazes have affected observations of exoplanet atmospheres with the *Hubble* and *Spitzer* space telescopes by muting signatures of molecular features in transmission (Kreidberg et al. 2014; Sing et al. 2016; Crossfield & Kreidberg 2017). If clouds or hazes are present at the planetary limb, they pose a problem for transmission spectra of terrestrial exoplanets because of long path lengths through the atmosphere (Moran et al. 2018; Afrin Badhan et al. 2019; Fauchez et al. 2019; Lustig-Yaeger et al. 2019).

Surface liquid water is considered a necessary constituent of a habitable world (Kasting et al. 1993), and ideally we would like to detect water vapor spectral signatures as an indicator of the habitability of a terrestrial exoplanet. Given the narrow thermodynamic range of liquid water stability, and typical lapse rates in planetary atmospheres, any planet with abundant liquid surface water will also have clouds condensing in its atmosphere. This suggests that hunting for water spectral

signatures will be confounded by clouds in terrestrial planet atmospheres. On tidally locked planets with hot daysides and cold nightsides, upwelling on the dayside carries moist air to low pressures. This moist air condenses as it is lifted, leading to strong dayside cloud cover on tidally locked terrestrial planets that have surface water (Yang et al. 2013, 2019a; Kopparapu et al. 2017; Haqq-Misra et al. 2018; Fauchez et al. 2019; Komacek & Abbot 2019; Suissa et al. 2019). If this dayside cloud cover extends to the terminator, it could significantly hinder the detection of molecular features in transmission.

Recent climate modeling has begun to explore how clouds affect the detection of transmission spectral features with *JWST*. Using the 1D climate and photochemical models of Lincowski et al. (2018), Lustig-Yaeger et al. (2019) found that clouds inhibit the detection of water features on TRAPPIST-1e. However, 3D simulations are necessary to accurately simulate cloud and water vapor mixing ratios. By post-processing 3D general circulation model (GCM) experiments, Fauchez et al. (2019) and Suissa et al. (2019) found that water vapor is challenging to detect in the atmospheres of terrestrial planets in the habitable zone due to the presence of clouds. However, Fauchez et al. (2019) analyzed simulations only varying the atmospheric composition for individual planets in the TRAPPIST-1 system, and Suissa et al. (2019) considered only the joint effects of varying incident stellar flux and rotation period.

In this work, we consider how a much broader range of possible planetary parameters affects transmission spectra. To do so, we post-process the 3D GCM output of Komacek &

Abbot (2019) to make simulated *JWST* observations of transmission spectra for planets orbiting late-type M dwarf stars. We find that clouds make water vapor transmission spectral features challenging to detect with *JWST* over a wide range of planetary parameters. We study the difference in transmission spectra when including and not including clouds, along with the effects of varying rotation rate, incident stellar flux, surface pressure, planetary radius, surface gravity, and cloud particle size. In Section 2, we describe our GCM experiments and how we post-process our GCM results to simulate transmission spectra. We show how clouds and varying planetary parameters impact transmission spectra in Section 3, along with estimating the number of transits needed to detect water vapor transmission features with *JWST*. We discuss our results and conclude in Section 4.

2. Methods

2.1. GCM Setup

To simulate the atmospheres of tidally locked terrestrial exoplanets, we use the EXOCAM GCM⁷ (Wolf & Toon 2015). EXOCAM is a version of the Community Atmosphere Model version 4 with updated correlated-k radiative transfer and water vapor continuum absorption, with spectral coefficients from HITRAN 2012. EXOCAM has been used in a wide range of studies of the atmospheres of terrestrial exoplanets (Kopparapu et al. 2016, 2017; Wolf et al. 2017, 2019; Wolf 2017; Haqq-Misra et al. 2018; Komacek & Abbot 2019; Yang et al. 2019a). We vary the rotation period, surface pressure, incident stellar flux, planetary radius, surface gravity, and cloud particle size over a wide range relevant for terrestrial exoplanets. The first column of Table 1 shows our considered variations in planetary parameters. Specifically, we use the GCM results for planets orbiting a late-type M dwarf star with $T_{\text{eff}} = 2600$ K from Komacek & Abbot (2019, see their Table 3). We conduct additional simulations to cover a range of dynamical regimes, including fast, intermediate, and slow rotators. If it is not explicitly stated in Table 1 that a parameter is varied, we keep its value fixed to that of Earth. As a result, this suite of GCM experiments varies planetary parameters individually, and includes some combinations of rotation period and incident stellar flux that are inconsistent with Kepler’s laws. We analyze these simulations in order to examine how each of these factors individually affect transmission spectra.

We consider an atmosphere consisting of only N_2 and H_2O on a tidally locked aquaplanet with a 50 m deep slab ocean and zero obliquity. As a result, in this work we focus on how clouds and varying planetary parameters affect transmission spectra. We conducted additional GCM experiments including Earth-like abundances of CO_2 and CH_4 in order to test the sensitivity of our results to additional greenhouse gases. To determine if the parameterized ice cloud particle size in EXOCAM affects our results, we also include a suite of sensitivity tests with varying ice cloud particle size. Our range of considered ice cloud particle size is 20–200 μm (see Table 2), chosen to cover the range of ice cloud particle size in the parameterization of Rasch & Kristjánsson (1998) used in EXOCAM. All simulations use a horizontal resolution of $4^\circ \times 5^\circ$ with 40 vertical levels and a timestep of 30 minutes. The GCM results presented in this work are averaged over the last 10 yr of simulation time.

⁷ <https://github.com/storyofthewolf/ExoCAM>

Table 1
Clouds Dramatically Increase the Number of Transits Needed to Detect Water Features

Simulation Parameters	Number of Transits with Clouds	Number of Transits Ignoring Clouds
Rotation Period		
1 day	>1000	71
2 days	658	18
4 days	180	10
8 days	63	4
16 days	189	2
Surface Pressure		
1 day rotation period:		
0.5 bars	>1000	52
1 bar	>1000	71
2 bars	>1000	67
4 bars	>1000	174
8 day rotation period:		
0.5 bars	24	2
4 bars	54	2
16 day rotation period:		
0.5 bars	68	1
4 bars	12	1
Planetary Radius		
1 day rotation period:		
0.5 R_\oplus	>1000	535
0.707 R_\oplus	>1000	202
1 R_\oplus	>1000	71
1.414 R_\oplus	>1000	32
2 R_\oplus	250	6
8 day rotation period:		
0.5 R_\oplus	>1000	11
2 R_\oplus	>1000	1
16 day rotation period:		
0.5 R_\oplus	904	5
2 R_\oplus	10	1
Surface Gravity		
1 day rotation period:		
0.707 g_\oplus	>1000	28
1 g_\oplus	>1000	71
1.414 g_\oplus	>1000	149
8 day rotation period:		
0.707 g_\oplus	479	1
1.414 g_\oplus	187	4
16 day rotation period:		
0.707 g_\oplus	27	1
1.414 g_\oplus	299	2
Incident Stellar Flux and Rotation Period		
0.544 F_\oplus , 6.49 days	616	83
0.667 F_\oplus , 5.57 days	>1000	69
0.816 F_\oplus , 4.79 days	709	43
1 F_\oplus , 4.11 days	320	10

Note. Shown are the number of transits needed to detect water features at an $S/N \geq 5$ with and without clouds for planets orbiting a late-type M dwarf star with $T_{\text{eff}} = 2600$ K using *JWST* NIRSpec/Prism.

2.2. Simulated Observables

To simulate transmission spectra from our GCM output, we use the Planetary Spectrum Generator⁸ (PSG; Villanueva et al.

⁸ <https://psg.gsfc.nasa.gov>

Table 2

Transmission Spectral Features of Water are Challenging to Detect over a Wide Range of Cloud Particle Size

Ice Cloud Particle Radius	Number of Transits
20 μm	126
50 μm	378
80 μm	377
110 μm	434
140 μm	327
170 μm	297
200 μm	222

Note. Shown are the number of transits needed to detect water features at an $S/N \geq 5$ with ice clouds of varying particle size. These experiments have a rotation period of 16 days and all other parameters are fixed to that of Earth.

2018). We use the moderate spectral resolution mode of PSG, which employs the correlated-k technique for radiative transfer, while multiple scattering from aerosols is performed using the discrete ordinates method. The molecular spectroscopy is based on the HITRAN 2016 database (Gordon et al. 2017), which is complemented by ultraviolet (UV)/optical data from the MPI-Mainz database (Keller-Rudek et al. 2013). We take the temperature, molecular abundance, and liquid and ice cloud profiles from the GCM at each latitude point on the limb as input for PSG. We then use PSG to make a simulated transmission spectrum at every GCM grid point along the terminator, each of which comprises 4° of latitude. To make the planetary transmission spectrum, we average the spectra over all latitudinal grid points along the terminator with equal weighting of each spectrum, the same method as used in Fauchez et al. (2019) and Suissa et al. (2019). Note that this method only takes into account transmission through the limb, but transmission through the cloudier dayside may further reduce the amplitude of transmission spectral features (Caldas et al. 2019).

We simulate the transmission spectra for $R = 300$ from 0.6 to $5.3 \mu\text{m}$ relevant for the Near-Infrared Spectrograph (NIRSpec)/PRISM instrument on *JWST*, which has been shown to be the ideal instrument for *JWST* characterization of terrestrial exoplanets (Batalha et al. 2018; Fauchez et al. 2019; Lincowski et al. 2019; Lustig-Yaeger et al. 2019). We use the PSG imager noise model and do not include a noise floor in our simulated spectra. As a result, our results can be considered lower limits on the number of required transits to detect water vapor. Note that Suissa et al. (2019) showed that including a noise floor greatly affects the detectability of water features, finding that water vapor is not detectable if the *JWST* noise floor is ≥ 5 ppm.

3. The Dependence of Transmission Spectra on Planetary Parameters

3.1. Transmission Spectra with and without Clouds

Our simulated transmission spectra depend strongly on whether we include clouds. Figure 1 shows simulated transmission spectra from 30 transits with *JWST* NIRSpec/PRISM. We show results from two GCM experiments with rotation periods of 8 and 16 days, simulating the transmission spectra both including and not including the effects of clouds. We find that when we do not include the effects of clouds in our simulated transmission spectra, transmission spectral features are deep and well above the level of the noise.

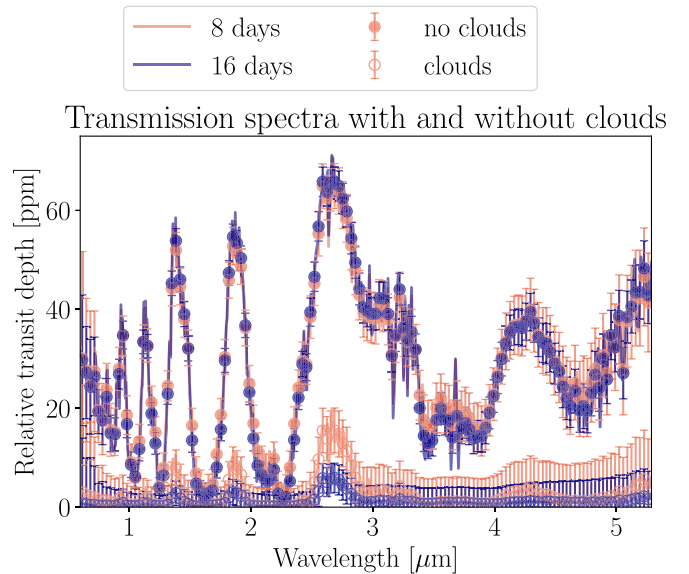


Figure 1. Clouds truncate spectral features. Simulated transmission spectra ignoring clouds (filled points) and including clouds (empty points) for planets with a rotation period of 8 days (orange) and 16 days (blue) orbiting a late-type M dwarf star. Lines show simulated spectra from 30 transits with *JWST* NIRSpec/PRISM, while points with 1σ errorbars show simulated observations binned to $R = 30$. A transit depth of zero corresponds to the continuum level of the planetary transmission, and the relative transit depth corresponds to the depth of features relative to the continuum. All of the absorption features are due to water except for the $4.1 \mu\text{m}$ feature, which is due to $\text{N}_2\text{-N}_2$ collision-induced absorption. When we include clouds, transmission spectral features of water are significantly diminished. Transmission features are especially weak for planets with long rotation periods.

However, when we include the effects of clouds, the transmission spectral features are strongly muted, with a maximum depth of ~ 20 ppm that is comparable to the expected noise floor of *JWST* NIRSpec (Greene et al. 2016).

Cloud muting of transmission spectral features is particularly strong for slowly rotating planets. In Figure 1, spectral features for the case with a rotation period of 16 days have an amplitude less than half that of the 8 day rotation period case. Figure 2 shows the liquid and ice cloud condensate at the terminator for the 8 and 16 day rotation period cases. As in Haqq-Misra et al. (2018), we find in that there is a greater amount of high-altitude ice cloud condensate in our more slowly rotating simulations. The increase in high-altitude ice cloud condensate leads to the more strongly muted spectral features in the 16 day rotation period case.

3.2. Detectability of Molecular Features

Table 1 shows how the number of transits needed to detect water vapor with *JWST* NIRSpec/PRISM depends on planetary parameters, both including and not including the effect of clouds. We assume that a signal-to-noise ratio (S/N) of 5 is required for detection. We determine the number of transits required to reach a given S/N using the method of Lustig-Yaeger et al. (2019), assuming that the S/N scales with the square root of the number of transit events. We perform this calculation for the maximum S/N of any water feature in the NIRSpec/PRISM bandpass, but note that the results are similar when considering the $1.4 \mu\text{m}$ water feature (which does not overlap with a CO_2 feature) alone.

Because TRAPPIST-1 is not continuously visible, Lustig-Yaeger et al. (2019) find that *JWST* will have 123 opportunities

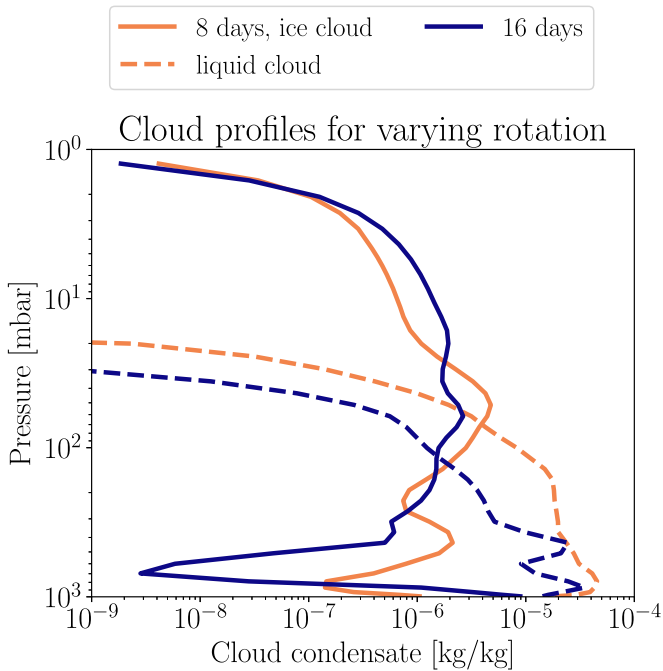


Figure 2. Rotation can greatly impact cloud coverage. Ice cloud condensate (solid lines) and liquid cloud condensate (dashed lines) from EXOCAM simulations of a planet with a rotation period of 8 days (orange) and 16 days (blue) orbiting a late-type M dwarf star, with all other parameters fixed to that of Earth. Profiles are averaged along the terminator. We find an increase in the high ice cloud cover between rotation periods of 8 and 16 days, leading to weaker water vapor absorption features.

in its nominal 5 yr lifetime to observe the transit of TRAPPIST-1d, which has an orbital period of 4.05 days. Assuming the same visibility as TRAPPIST-1, the number of observable transits would decrease to 31 for a planet with an orbital period of 16 days. Note that this is the maximum observable number of transits, and a realistic *JWST* observing strategy would likely not capture every transit event. For our optimistic case of an Earth-sized planet with an 8 day rotation period, 62 transits are observable over the *JWST* lifetime, similar to the 63 needed to detect water vapor if its surface pressure is equal to that of Earth (see Table 1).

We find that, ignoring clouds, only ~ 10 transits would be required to detect water vapor in the atmosphere of a terrestrial exoplanet that orbits a late-type M dwarf star and receives an incident flux equal to that of Earth. The number of transits needed to detect water vapor decreases with increasing rotation period. This is because more slowly rotating planets orbiting M dwarf stars have increased dayside convergence, leading to enhanced vertical transport of water vapor (Komacek & Abbot 2019). When we include water clouds, the number of transits needed to detect water features is one to two orders of magnitude greater than when we do not include water clouds, for all considered variations in planetary parameters. We find that 63 or more transits are required to detect water vapor in the atmospheres of Earth-sized planets with 1 bar atmospheres in the habitable zone around late-type M dwarf stars.

Figure 3 shows how the number of transits needed to detect water depends on rotation period in our suite of simulations. We find that the number of transits needed to detect water vapor sharply increases from 63 to 189 transits with increasing rotation period from 8 to 16 days. When not including clouds, $\lesssim 10$ transits are required to detect water vapor for planets with

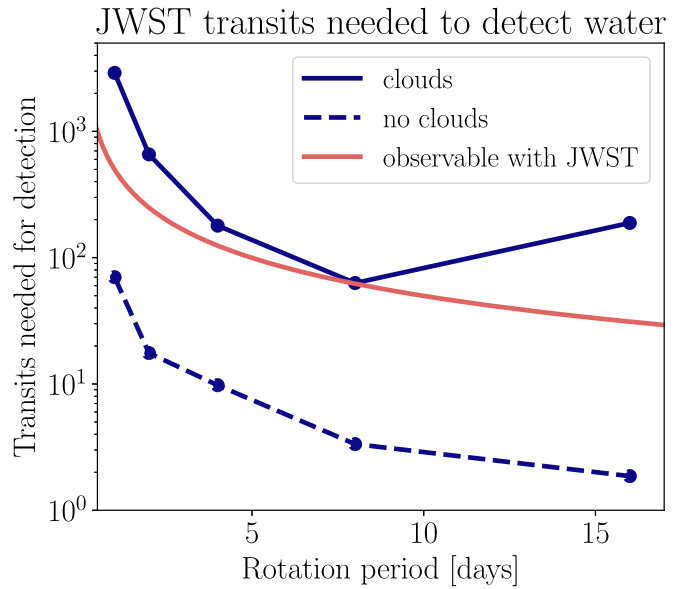


Figure 3. Clouds increase the number of transits needed to detect water vapor by one to two orders of magnitude. Number of transits needed to detect water features both including and not including the effects of clouds from simulations with varying rotation period are shown in blue. The maximum number of transits observable with *JWST* for varying rotation period is shown in red, assuming the visibility of TRAPPIST-1 and synchronous rotation. Points show individual simulations for varying rotation period including clouds (solid lines connecting points) and not including clouds (dashed lines).

rotation periods ≥ 4 days. As a result, we expect that clouds will cause water vapor features to be challenging to detect in the atmospheres of Earth-sized planets with *JWST*. However, an extended mission lifetime, lowered S/N threshold for detection, or the discovery of a habitable planet that is continuously visible to *JWST* may allow for a detection of water vapor.

3.3. Dependence of Water Vapor Detection on Planetary and Atmospheric Properties

Table 1 shows that the number of transits needed to detect water vapor is extremely sensitive to planetary parameters. We find that rotation period is a key controlling parameter. This is because planets that rotate quickly have reduced transport of water vapor to high altitudes, while planets that rotate slowly have significant high-altitude cloud cover at the terminator. When varying incident stellar flux and rotation period together, we find that there is a maximum in the number of transits needed to detect water vapor at an intermediate rotation period of 5.57 days. This is because there is a dynamical transition leading to decreased cloud cover for planets that are closer to their host star and more rapidly rotating (Komacek & Abbot 2019), reducing the number of transits needed to detect water vapor. When varying surface pressure alone in the rapidly rotating regime and ignoring the effect of clouds, we find that the number of transits required to detect water vapor sharply increases with increasing surface pressure from 2 to 4 bars. This is because Rayleigh scattering from atmospheric N_2 increases with increasing surface pressure (Kopparapu et al. 2014), leading to a cooler climate and reduced atmospheric water vapor content (Komacek & Abbot 2019).

In our simulations with a rotation period of 16 days, planets have ubiquitous high ice cloud coverage over a wide range of planetary parameters. Within this slowly rotating regime, we

find that planets that have larger radii, have lower gravities, and/or have higher surface pressures require fewer transits to detect water features. This is because, for fixed gravity, larger planets have a larger total transit signal, making deviations from the total signal larger. For fixed radius, lower-gravity planets have larger scale heights, leading to larger transmission features. Increasing the surface pressure leads to an increase in global-mean temperature and water vapor content of the air, leading to larger transmission features. The combination of large radius, high surface pressure, and low gravity enhances the detectability of water. Our results hence point toward sub-Neptunes (e.g., K2-18b, Benneke et al. 2019; Tsiaras et al. 2019) as viable targets to search for water vapor in transmission.

In simulations with an intermediate rotation period of 8 days, we find that the cloud coverage is itself strongly affected by planetary parameters. The resulting trends in the number of transits needed to detect water are non-monotonic with increasing surface pressure, radius, and gravity. Higher surface pressure leads to a cloudier dayside (Komacek & Abbot 2019), which increases the number of transits needed to detect water. However, at high surface pressures the increased amount of water vapor in the atmosphere makes it easier to detect. Larger radius leads to an increase in the size of transmission features, but at $2 R_{\oplus}$ we find a transition to a more rapidly rotating dynamical regime (Yang et al. 2019a) that increases high-altitude ice cloud coverage and diminishes spectral features. Increased surface gravity makes the atmosphere clearer by causing the settling rate of cloud particles to increase. This is counteracted by the reduced atmospheric scale height of planets with larger gravity, making water hard to detect on high-gravity planets.

Our results are robust over a wide range in cloud particle size. Table 2 shows how the number of transits needed to detect water vapor on slowly rotating terrestrial exoplanets orbiting late-type M dwarf stars depends on the ice cloud particle size. We find that for slowly rotating planets with otherwise Earth-like planetary parameters, no cloud particle size that we consider allows detection of water vapor in fewer than 100 transits, over a factor of 10 variation in ice cloud particle size. Still, our results underly the importance of accurate micro-physical modeling of cloud particle sizes, as plausible changes in ice cloud particle size can change the number of transits required for water detection by more than a factor of three. Additionally, we performed sensitivity tests including 400 ppm of CO_2 and 1.7 ppm of CH_4 in our GCM simulations. We found that the number of transits needed to detect water vapor when including CO_2 and CH_4 is comparable to or greater than that in simulations without CO_2 and CH_4 .

4. Discussion and Conclusions

Our results are consistent with Lustig-Yaeger et al. (2019), Fauchez et al. (2019), and Suissa et al. (2019), who also found that clouds will probably prevent the detection of water features on terrestrial planets via transit spectroscopy with *JWST*. These results are also consistent with the non-detection of molecular features in the atmospheres of TRAPPIST-1d, e, and f with the *Hubble Space Telescope* (de Wit et al. 2018). However, water clouds only affect features originating from below the cloud deck, so well-mixed species that have strong spectral features (e.g., CO_2 , CH_4) may still be detectable in the presence of water clouds (Fauchez et al. 2019). As a result, searching for

chemical disequilibrium as an exoplanet biosignature (Krisansen-Totton et al. 2018a, 2018b) would likely not be significantly impacted by the presence of clouds. Similarly, a statistical search for variations in CO_2 as a function of position in the habitable zone might still be possible (Bean et al. 2017).

In this work, we did not consider atmospheres of planets that have significant amounts of water in the stratosphere or that are too hot to have surface liquid water. Fujii et al. (2017) showed that atmospheres in a moist greenhouse state have strong water vapor spectral features. Further, Chen et al. (2019) found that transmission spectral features of water vapor in these atmospheres could be detectable with *JWST*. Due to the increased scale height of runaway greenhouse atmospheres (Turbet et al. 2019), observations of the atmospheres of terrestrial exoplanets orbiting M dwarfs that are interior to the habitable zone should find stronger molecular signatures.

Though we post-processed a complex GCM to simulate transmission spectra over a wide range of planetary parameters, there are a variety of limitations to our model setup. We did not consider all atmospheric constituents relevant for Earth-like planets, including O_2 and O_3 . Additionally, we did not perform a retrieval on simulated spectra to quantify the effects of band overlap between molecular species on detectability. We did not include a dynamic ocean, which would affect the surface temperature distribution and location of dayside cloud cover (Hu & Yang 2014; Del Genio et al. 2019; Way et al. 2018; Yang et al. 2019b). We did not include continents, which could reduce the amount of water vapor available to form clouds (Lewis et al. 2018). Lastly, we assumed that water is plentiful on the surfaces of planets orbiting M dwarf stars. It is possible that planets orbiting M dwarf stars lose their entire surface complement of water, leading to high amounts of O_2 that could act as a false-positive biosignature (Ramirez & Kaltenegger 2014; Luger & Barnes 2015; Raff 2015; Schaefer et al. 2016).


In this work, we quantified the effect of water clouds on transmission spectra of tidally locked terrestrial exoplanets with a range of planetary parameters in the habitable zone of M dwarf stars. We find that transmission spectral features of water are significantly muted due to clouds on terrestrial exoplanets orbiting M dwarf stars. The decrease in transit depth due to clouds is especially strong for slowly rotating planets with rotation periods $\gtrsim 12$ days, which have large dayside cloud decks. Due to cloud coverage, water transmission features of Earth-sized planets orbiting M dwarf stars will be challenging to detect with *JWST*.

We thank the referee for thoughtful comments that improved the manuscript. We acknowledge support from the NASA Astrobiology Institutes Virtual Planetary Laboratory, which is supported by NASA under cooperative agreement NNNH05ZDA001C. T.D.K. acknowledges funding from the 51 Pegasi b Fellowship in Planetary Astronomy sponsored by the Heising-Simons Foundation. Our work was completed with resources provided by the University of Chicago Research Computing Center.

ORCID iDs

Thaddeus D. Komacek  <https://orcid.org/0000-0002-9258-5311>

Thomas J. Fauchez  <https://orcid.org/0000-0002-5967-9631>

Eric T. Wolf  <https://orcid.org/0000-0002-7188-1648>

Dorian S. Abbot  <https://orcid.org/0000-0001-8335-6560>

References

- Afrin Badhan, M., Wolf, E., Kopparapu, R., et al. 2019, *ApJ*, **887**, 34
- Barstow, J., & Irwin, P. 2016, *MNRAS*, **461**, L92
- Batalha, N. E., Lewis, N. K., Line, M. R., Valenti, J., & Stevenson, K. 2018, *ApJL*, **856**, L34
- Bean, J. L., Abbot, D. S., & Kempton, E. M.-R. 2017, *ApJL*, **841**, L24
- Benneke, B., Wong, I., Piaulet, C., et al. 2019, *ApJL*, **887**, L14
- Caldas, A., Leconte, J., Selsis, F., et al. 2019, *A&A*, **623**, A161
- Chen, H., Wolf, E. T., Zhang, Z., & Horton, D. E. 2019, *ApJ*, **886**, 16
- Crossfield, I., & Kreidberg, L. 2017, *AJ*, **154**, 261
- de Wit, J., Wakeford, H., Lewis, N., et al. 2018, *NatAs*, **2**, 214
- Del Genio, A., Way, M., Amundsen, D., et al. 2019, *AsBio*, **19**, 99
- Faucher, T. J., Turbet, M., Villanueva, G. L., et al. 2019, *ApJ*, **887**, 194
- Fujii, Y., Genio, A. D., & Amundsen, D. 2017, *ApJ*, **848**, 100
- Gordon, I. E., Rothman, L. S., Hill, C., et al. 2017, *JQSRT*, **203**, 3
- Greene, T., Line, M., Montero, C., et al. 2016, *ApJ*, **817**, 17
- Haqq-Misra, J., Wolf, E., Josh, M., Zhang, X., & Kopparapu, R. 2018, *ApJ*, **852**, 67
- Hu, Y., & Yang, J. 2014, *PNAS*, **111**, 629
- Kasting, J. F., Whitmire, D. P., & Reynolds, R. T. 1993, *Icar*, **101**, 108
- Keller-Rudek, H., Moortgat, G. K., Sander, R., & Sørensen, R. 2013, *ESSD*, **5**, 365
- Komacek, T., & Abbot, D. 2019, *ApJ*, **871**, 245
- Kopparapu, R. K., Ramirez, R. M., SchottelKotte, J., et al. 2014, *ApJL*, **787**, L29
- Kopparapu, R. K., Wolf, E., Arney, G., et al. 2017, *ApJ*, **845**, 5
- Kopparapu, R. K., Wolf, E., Haqq-Misra, J., et al. 2016, *ApJ*, **819**, 84
- Kreidberg, L., Bean, J. L., Désert, J.-M., et al. 2014, *Natur*, **505**, 69
- Krissansen-Totton, J., Garland, R., Irwin, P., & Catling, D. C. 2018a, *AJ*, **156**, 114
- Krissansen-Totton, J., Olson, S., & Catling, D. C. 2018b, *SciA*, **4**, 5747
- Lewis, N., Lambert, F., Boutle, I., et al. 2018, *ApJ*, **854**, 171
- Lincowski, A., Lustig-Yaeger, J., & Meadows, V. 2019, *AJ*, **158**, 26
- Lincowski, A., Meadows, V., Crisp, D., et al. 2018, *ApJ*, **867**, 76
- Luger, R., & Barnes, R. 2015, *AsBio*, **15**, 119
- Lustig-Yaeger, J., Meadows, V., & Lincowski, A. 2019, *AJ*, **158**, 27
- Moran, S. E., Hörst, S. M., Batalha, N. E., Lewis, N. K., & Wakeford, H. R. 2018, *AJ*, **156**, 252
- Morley, C., Kreidberg, L., Rustamkulov, Z., Robinson, T., & Fortney, J. 2017, *ApJ*, **850**, 121
- Raff, J. 2015, *NatGe*, **8**, 5
- Ramirez, R. M., & Kaltenegger, L. 2014, *ApJL*, **797**, L25
- Rasch, P., & Kristjánsson, J. 1998, *JCLI*, **11**, 1587
- Schaefer, L., Wordsworth, R., Berta-Thompson, Z., & Sasselov, D. 2016, *ApJ*, **829**, 63
- Sing, D. K., Fortney, J. J., Nikolov, N., et al. 2016, *Natur*, **529**, 59
- Suissa, G., Mandell, A. M., Wolf, E. T., et al. 2019, *ApJ*, submitted (arXiv:1912.08235)
- Tsiaras, A., Waldmann, I. P., Tinetti, G., Tennyson, J., & Yurchenko, S. N. 2019, *NatAs*, **3**, 1086
- Turbet, M., Ehrenreich, D., Lovis, C., Bolmont, E., & Faucher, T. 2019, *A&A*, **628**, A12
- Villanueva, G., Smith, M., Protopapa, S., Faggi, S., & Mandell, A. 2018, *JQSRT*, **217**, 86
- Way, M., Genio, A. D., Aleinov, I., et al. 2018, *ApJS*, **239**, 24
- Wolf, E. 2017, *ApJL*, **839**, L1
- Wolf, E., Kopparapu, R., & Haqq-Misra, J. 2019, *ApJ*, **877**, 35
- Wolf, E., Shields, A., Kopparapu, R., Haqq-Misra, J., & Toon, O. 2017, *ApJ*, **837**, 107
- Wolf, E., & Toon, O. 2015, *JGRD*, **120**, 5775
- Yang, H., Komacek, T., & Abbot, D. 2019a, *ApJL*, **876**, L27
- Yang, J., Abbot, D., Koll, D., Hu, Y., & Showman, A. 2019b, *ApJ*, **871**, 29
- Yang, J., Cowan, N., & Abbot, D. 2013, *ApJL*, **771**, L45